

Cosmological Time Dilation in Durations of *Swift* Long Gamma-Ray Bursts

Fu-Wen Zhang^{1,2}, Yi-Zhong Fan¹, Lang Shao³ and Da-Ming Wei¹

ABSTRACT

Cosmological time dilation is a fundamental phenomenon in an expanding universe, which stresses that both the duration and wavelength of the emitted light from a distant object at the redshift z will be dilated by a factor of $1 + z$ at the observer. By using a sample of 139 *Swift* long GRBs with known redshift ($z \leq 8.2$), we measure the observed duration (T_{90}) in the observed energy range between $140/(1 + z)$ keV and $350/(1 + z)$ keV, corresponding to a fixed energy range of 140-350 keV in the rest frame. We obtain a significant correlation between the duration and the factor $1 + z$, i.e., $T_{90} = 10.5(1 + z)^{0.94 \pm 0.26}$, which is well consistent with that expected from cosmological time dilation effect.

Subject headings: gamma-rays burst: general - methods: data analysis

1. INTRODUCTION

Gamma-ray bursts (GRBs) are the most violent explosions in distant galaxies (Piran 2004; Zhang & Mészáros 2004). The search for the cosmological time dilation signature in GRB data, a fundamental phenomenon in an expanding universe, has a long history. In the pre-*Swift*-era, the verification of time dilation signature in GRB data was in heavy debate (Norris et al. 1994; Che et al. 1997a,b; Lee & Petrosian 1997; Deng & Schaefer 1998; Lee et al. 2000; Mitrofanov et al. 1996; Chang 2001; Chang et al. 2002; Borgonovo 2004; Norris 2002; Bloom et al. 2003; Wei & Gao 2003). The main uncertainty of these early results is that these samples contained small or even zero number of bursts with known redshift. Thanks to the successful performance of *Swift* satellite (Gehrels et al. 2004), the number of GRBs with measured redshift increases rapidly and a reliable test of the time dilation signature reported in previous literature becomes possible. Nevertheless, recent analyses still revealed no sound evidence for the cosmological time dilation effect in GRBs

¹Key Laboratory of Dark Matter and Space Astronomy, Purple Mountain Observatory, Chinese Academy of Sciences, Nanjing 210008, China

²College of Science, Guilin University of Technology, Guilin 541004, China

³Department of Physics, Hebei Normal University, Shijiazhuang 050016, China

detected by *Swift* or Fermi Gamma-ray Telescope (Sakamoto et al. 2011; Kocevski & Petrosian 2013; Gruber et al. 2011).

It is well known that the intrinsic durations or light curves of GRBs are highly energy dependent (Fenimore et al. 1995; Norris et al. 1996; Peng et al. 2006; Zhang et al. 2007; Zhang 2008; Zhang et al. 2012; Qin et al. 2013). We note that most previous works ignored this effect and simply measured the observed durations in a fixed observed energy range. As a result, the received photons belong to different energy ranges when emitted in the rest frame of different GRBs. Therefore, the observed durations would be strongly biased since they simply recorded different parts of the intrinsic light curves. This can be settled by choosing a fixed energy range in the rest frame and measuring the observed duration in a projected energy range by the relation $E_{\text{obs}} = E_{\text{rest}}/(1 + z)$, where E_{obs} and E_{rest} are the energy of the photon measured in the observer and the rest frame, respectively (Sakamoto et al. 2011; Gruber et al. 2011; Ukwatta et al. 2012). When taking this effect into account, we calculate the observed durations of *Swift* GRBs with known redshifts within the observed energy band $140/(1 + z)$ keV to $350/(1 + z)$ keV, corresponding to the same rest frame energy range 140-350 keV, and reanalyze the redshift dependence of the durations. We find that there is a significant trend that the inferred duration tend to be longer in bursts at higher redshifts and the durations are stretched approximately by a factor $(1 + z)$, as expected from cosmological time dilation effect. We describe our sample and data analysis in section 2, present the results in Section 3, and give our conclusions in Section 4.

2. Sample and data analysis

In order to obtain a complete sample and minimize the influence of different instruments (with different sensitivities and energy bands), only *Swift* GRBs with known redshift are considered. We obtain a sample of 194 bursts with known redshift¹ detected by March, 2012. We download the data from *Swift* Archive available at <ftp://legacy.gsfc.nasa.gov/swift/data/>. The time tagged event (TTE) data from Burst Alert Telescope (BAT) onboard *Swift* have excellent time resolution of 100 μs , which can be used to perform the temporal analysis well. The standard BAT software (HEASOFT 6.8) and the latest calibration database are used to process the BAT TTE data. We extract 64 ms (long bursts) or 16 ms (short bursts) binned light curve from the TTE data and determine the GRB duration, T_{90} (T_{50}), by the time in which 90% (50%) of the burst counts are collected (Kouveliotou et al. 1993). The widely used Bayesian Block method (Scargle 1998) is adopted to extract the duration value.

¹<http://www.mpe.mpg.de/~jcg/grbgen.html>

Using the standard method described above, we firstly calculate the values of $T_{90,\text{raw}}$ and $T_{50,\text{raw}}$, where the subscript “raw” represents the data measured in the observer’s energy range of 15 – 350 keV. These duration values are generally used in previous studies. But the statistical analysis of $T_{90,\text{raw}}$ and $T_{50,\text{raw}}$ is somehow meaningless or even misleading, because the values of $T_{90,\text{raw}}$ and $T_{50,\text{raw}}$ are highly affected by both the energy-dependent effect and the cosmological time-dilation effect. By fixing the energy range in the GRB rest frame, the energy-dependent effect is removed. We then created the light curves in the observed energy range $140/(1+z)$ keV to $350/(1+z)$ keV. This energy band was chosen so that the projecting energy bands of all *Swift* GRBs with known redshifts lie in the *Swift*-BAT observed energy range (15-350 keV). We used the same algorithm to find the best T_{90} and T_{50} durations in the observed $140/(1+z)$ - $350/(1+z)$ keV band. The rest frame durations $T_{90,\text{rest}}$ and $T_{50,\text{rest}}$ can be easily obtained by dividing the observed durations by $(1+z)$.

In our initial sample of 194 GRBs, some bursts are not bright enough to measure T_{90} and T_{50} in the rest frame energy range 140 – 350 keV. Six super-long/peculiar bursts (GRBs 060124, 060218, 100316D, 101225A, 110328A, 111209A) are excluded in our investigation. In the analysis we also exclude the short duration bursts, including two with extended emission (GRBs 060614 and 061210). Please note the short and long duration bursts (≤ 2 s) are defined following Kouveliotou et al. (Kouveliotou et al. 1993)², not by the T_{90} measured in this work. The benefit of excluding them is to have a sample of GRBs that have an intrinsically same (or similar) duration distribution. Our analysis is thus based on a *Swift* GRB sample consisting of 139 long GRBs. In addition, three very high redshift candidates (GRBs 090429B, 120521C and 120923A) are also presented for comparison.

3. Relation between duration and redshift

Assuming that the intrinsic duration of all GRBs is similar, one would expect the observed duration to increase as a function of redshift due to the cosmological expansion. As shown in Fig.1, there is a clear trend that farther bursts tend to have larger T_{90} and T_{50} . We parameterize the correlation and obtain $\log T_{90} = (1.02 \pm 0.14) + (0.94 \pm 0.26) \log(1+z)$, where the Pearson correlation coefficient is $r = 0.29$ and the chance probability is $p = 0.0005$. For T_{50} , we have $\log T_{50} = (0.58 \pm 0.14) + (1.07 \pm 0.27) \log(1+z)$ with $r = 0.32$ and $p = 0.0001$. Therefore the observed GRB durations are indeed stretched approximately by a factor of $(1+z)$, as expected from the cosmological time dilation effect. The scatter is large and particularly two very high

²Recently, Bromberg et al. (2013) suggested that the commonly used limit of 2 s is conservative and the division ≤ 0.8 is more suitable for *Swift*.

redshift GRBs (GRBs 080913A at $z = 6.7$ and 090423 at $z = 8.2$) and two high redshift candidates (GRBs 090429B at $z \sim 9.4$ and 120923A at $z \sim 8.5$) do not comply with the correlation well. This might be because the intrinsic duration is not the same for all bursts. Besides, Zhang et al. (2009) have showed that most GRBs with the highest redshifts seem to have rest-frame durations shorter than 2 s, yet still show multi-wavelength properties similar to most long GRBs. Recently, by the simulations, several groups found that the diminishing S/N of higher redshift GRBs makes only the bright narrow portions of the bursts accessible to the detectors (i.e., the so-called “tip-of-iceberg” effect), so the measured durations should be considered as lower limits to the true values (Kocevski & Petrosian 2013; Lv et al. 2012; Littlejohns et al. 2013).

To better show the correlation we divide the sample of 139 GRBs into six groups with almost equal number of bursts. We calculate the mean values of T_{90} , T_{50} and z in each groups and reanalyze their relations. From Fig.2 we find that the mean durations ($T_{90,\text{mean}}$, $T_{50,\text{mean}}$) are tightly correlated with the mean redshift z_{mean} . Fitting the correlation we have $\log T_{90,\text{mean}} = (1.28 \pm 0.10) + (0.97 \pm 0.19) \log(1+z_{\text{mean}})$ with $r = 0.93$ and $p = 0.007$, and $\log T_{50,\text{mean}} = (0.80 \pm 0.11) + (1.25 \pm 0.20) \log(1+z_{\text{mean}})$ with $r = 0.95$ and $p = 0.004$. Hence the $(1+z)$ stretching of durations is established. We have also analyzed the potential influence of the numbers of groups on the statistical result and found that the slope of the correlation is almost invariable and close to 1 for the different sets of groups. Although the intrinsic durations of individual bursts are very different, their mean value is dilated exactly by a factor of $1+z$ following the nature of the expanding universe (Paczynski 1992; Piran 1992).

Is the observed duration stretching due to the redshift evolution of the intrinsic duration of GRBs? To answer this question we also analyze the distribution of the rest frame duration $T_{90,\text{rest}}$ and $T_{50,\text{rest}}$ as well as the relation between these two quantities and redshift. From Fig.3, we find that the distributions of $T_{90,\text{rest}}$ and $T_{50,\text{rest}}$ all span a wide range and their log-median values are 10.7 s and 4.6 s, respectively. Obviously, different GRBs do not have a standard intrinsic duration. But, the similar median values of the intrinsic duration $T_{90,\text{rest}} \sim 10$ s have been reported by many authors even though different energy ranges and different instruments are engaged (Pélangéon et al. 2008; Shao et al. 2010; Gruber et al. 2011). Therefore, we can only identify the cosmological time dilation as a statistical effect. Fig.4 shows the redshift dependence of $T_{90,\text{rest}}$ and $T_{50,\text{rest}}$ and we do not find any evidence of the evolution effect of the rest frame duration, where the correlation coefficients (chance probabilities) between $T_{90,\text{rest}}$ and $T_{50,\text{rest}}$ and the redshifts are $r = -0.02$ ($p = 0.82$) and $r = 0.02$ ($p = 0.79$), respectively. A similar conclusion was also obtained from analyzing the preliminary Fermi/GBM data (Gruber et al. 2011).

It is well known that the duration of GRBs is highly affected by the detector threshold. In order to avoid the influence of the detector threshold on the correlation between duration and redshift, we construct a subsample with relatively bright bursts in the 15-150 keV Swift/BAT band. The

subsample is selected with the criteria that the bursts have 1-s peak photon flux $P \geq 2.6 \text{ ph s}^{-1} \text{ cm}^{-2}$ as done by Salvaterra et al.(2012). 63 GRBs match our selection criteria. We then analyze the relations between T_{90} , T_{50} and z (Fig. 5). From Fig. 5, we can find that the observed durations are highly depend on redshift for these bright GRBs, which is consistent with the above result. We parameterize the correlation and obtain $\log T_{90} = (0.87 \pm 0.20) + (1.07 \pm 0.45) \log(1 + z)$ with $r = 0.29$ and $p = 0.02$. For T_{50} , we have $\log T_{50} = (0.46 \pm 0.19) + (1.01 \pm 0.42) \log(1 + z)$ with $r = 0.29$ and $p = 0.02$. These results further confirm that the cosmological time dilation effect identified in the duration of GRBs is reliable.

Previous works in analyzing the data of *Swift* GRBs have reported no evidence for the duration being stretched by a factor of $(1 + z)$ (Sakamoto et al. 2011; Kocevski & Petrosian 2013), which seems to be at odds with our results. To check what happens, following previous approaches we also investigate the correlations between $T_{90,\text{raw}}$, $T_{50,\text{raw}}$ and z (Fig. 6). From Fig. 6, we find that there is indeed no evidence for the dilation-like effect in the raw duration data, in agreement with that found in previous studies. The respective correlation coefficients between $T_{90,\text{raw}}$ and $T_{50,\text{raw}}$ and the redshifts are $r = 0.03$ ($p = 0.69$) and $r = 0.13$ ($p = 0.13$). This suggests that the cosmological time dilation effect has been canceled by the energy-dependent effect of the duration, since the farther the burst is located, the shorter portion of the light curve (corresponding to a higher energy range in the rest frame) would be recorded in the observed energy range.

In addition, Pélangéon et al. (2008) and Kocevski & Petrosian (2013) found that the rest frame duration decrease as a function of redshift (see also Wei & Gao 2003). However, it should be noted that the rest frame duration used by these works only simply dividing the raw duration measured in a fixed detector energy range by a factor of $(1 + z)$, the energy-dependent effect is not considered. As a test, we also calculate $T_{90,\text{raw}}/(1 + z)$ and $T_{50,\text{raw}}/(1 + z)$ and analyze their relations with redshift. As shown in Fig. 7, both $T_{90,\text{raw}}/(1 + z)$ and $T_{50,\text{raw}}/(1 + z)$ all show a decreasing trend with increasing redshift. We parameterize the correlations and obtain $\log(T_{90,\text{raw}}/(1 + z)) = (1.65 \pm 0.13) + (-0.92 \pm 0.25) \log(1 + z)$ with $r = -0.3$ and $p = 0.0004$, and $\log(T_{50,\text{raw}}/(1 + z)) = (1.07 \pm 0.14) + (-0.64 \pm 0.27) \log(1 + z)$ with $r = -0.2$ and $p = 0.02$. Hence we have demonstrated that a reliable relation between the duration and the redshift can not be reliably established if one ignores the energy-dependent effect.

4. Summary and conclusions

In this work we perform a statistical analysis of the duration of a sample of 139 long GRBs with known redshift detected by *Swift* until March, 2012. We calculated the observed duration (T_{90} and T_{50}) of all bursts in the observed energy range $140/(1 + z)$ keV to $350/(1 + z)$ keV, which correspond to a fixed energy bands 140-350 keV in the rest frame. This actually means that the

energy-dependent effect is removed. By analyzing the relation between T_{90} , T_{50} and redshift, we find that there is a significant trend that both T_{90} and T_{50} tend to be longer in bursts at higher redshifts and $T_{90} = 10.5(1+z)^{0.94\pm 0.26}$ and $T_{50} = 3.8(1+z)^{1.07\pm 0.27}$. Such results are well consistent with that expected from cosmological time dilation effect that all timescales of GRBs should be stretched by a factor of $(1+z)$. We also find that the intrinsic duration of GRBs is independent with redshift and its distribution span a wide range, where the median value of $T_{90,\text{rest}}$ ($T_{50,\text{rest}}$) is 10.7 s (4.6 s), respectively. If one only uses the raw duration calculated within a fixed detector energy range to make the statistical analysis of duration, the result can be misleading. For example in some literature the “intrinsic duration” is found to be anti-correlated with the redshift, which is at odds with our finding. Hence a reliable relation between the duration and the redshift can not be reliably established if one ignores the energy-dependent effect of the duration.

We note that the correlation between duration and redshift has a very large scatter, this might be due to the intrinsic scatter in duration. A more important fact is that the several very high redshift GRBs deviate from the correlation. This might be caused by the integrated effect. A more important reason is the “tip-of-iceberg” effect that with increasing redshift and decreasing signal-to-noise ratio only the brightest portion of GRB light curves can be detected, so the measured durations should be considered as lower limits to the true values (Kocevski & Petrosian 2013; Lv et al. 2012; Littlejohns et al. 2013). In addition, the BAT effective area is not uniform, it sharply drops above 100 keV, and below 25 keV (Barthelmy et al. 2005; see also http://swift.gsfc.nasa.gov/analysis/bat_digest.html). This mainly affect the two extremes of the redshift distribution. The durations of low-redshift ($z < 1$) and highest-redshift ($z > 8$) events could therefore be also underestimated.

We thank the anonymous referee for the insightful comments/suggestions. This work was supported in part by the National Basic Research Program of China (No. 2014CB845800 and No. 2013CB837000) and the National Natural Science Foundation of China (grants 11163003, U1331101, 11073057, 11103083 and 11273063). Y.-Z.F. is also supported by the 100 Talents program of the Chinese Academy of Sciences and by the Foundation for Distinguished Young Scholars of Jiangsu Province, China (No. BK2012047). F.-W.Z. also acknowledges the support by the China Postdoctoral Science Foundation funded project (No. 20110490139), the Guangxi Natural Science Foundation (No. 2013GXNSFAA019002) and the doctoral research foundation of Guilin University of Technology.

REFERENCES

Barthelmy, S. D., Barbier, L. M., Cummings, J. R., et al. 2005, *Space Sci. Rev.*, 120, 143

- Borgonovo, L. 2004, *A&A*, 418, 487
- Bromberg, O., Nakar, E., Piran, T., & Sari, R. 2012, *ApJ*, 749, 110
- Bromberg, O., Nakar, E., Piran, T., & Sari, R. 2013, *ApJ*, 764, 179
- Bloom, J. S., Frail, D. A., & Kulkarni, S. R. 2003, *ApJ*, 594, 674
- Che, H., Yang, Y., Wu, M., & Li, Q. B. 1997a, *ApJ*, 483, L25
- Che, H., Yang, Y., Wu, M., & Li, T. P. 1997b, *ApJ*, 477, L69
- Chang, H.-Y. 2001, *ApJ*, 557, L85
- Chang, H.-Y., Yoon, S.-J., & Choi, C.-S. 2002, *A&A*, 383, L1
- Deng, M., & Schaefer, B. E. 1998, *ApJ*, 502, L109
- Fenimore, E. E., in't Zand, J. J. M., Norris, J. P., et al. 1995, *ApJ*, 448, L101
- Gehrels, N., Chincarini, G., Giommi, P., et al. 2004, *ApJ*, 611, 1005
- Kocevski, D., & Petrosian, V. 2013, *ApJ*, 765, 116
- Kouveliotou, C., Meegan, C. A., Fishman, G. J., et al. 1993, *ApJ*, 413, L101
- Lee, A., Bloom, E. D., & Petrosian, V. 2000, *ApJS*, 131, 21
- Lee, T. T., & Petrosian, V. 1997, *ApJ*, 474, 37
- Littlejohns, O. M., Tanvir, N. R., Willingale, R., et al. 2013, arXiv:1309.7045
- Lü, H.-J., Zhang, B., Liang, E.-W., et al. 2012, arXiv:1211.1117
- Mitrofanov, I. G., Chernenko, A. M., Pozanenko, A. S., et al. 1996, *ApJ*, 459, 570
- Norris, J. P. 2002, *ApJ*, 579, 386
- Norris, J. P., Nemiroff, R. J., Bonnell, J. T., et al. 1996, *ApJ*, 459, 393
- Norris, J. P., Nemiroff, R. J., Scargle, J. D., et al. 1994, *ApJ*, 424, 540
- Paczynski, B. 1992, *Nature*, 355, 521
- Pélangéon, A., Atteia, J.-L., Nakagawa, Y. E., et al. 2008, *A&A*, 491, 157
- Piran, T. 1992, *ApJ*, 389, L45

- Piran, T. 2004, *Reviews of Modern Physics*, 76, 1143
- Peng, Z.-Y., Qin, Y.-P., Zhang, B.-B., et al. 2006, *MNRAS*, 368, 1351
- Gruber, D., Greiner, J., von Kienlin, A., et al. 2011, *A&A*, 531, A20
- Qin, Y., Liang, E.-W., Liang, Y.-F., et al. 2013, *ApJ*, 763, 15
- Sakamoto, T., Barthelmy, S. D., Baumgartner, W. H., et al. 2011, *ApJS*, 195, 2
- Salvaterra, R., Campana, S., Vergani, S. D., et al. 2012, *ApJ*, 749, 68
- Scargle, J. D. 1998, *ApJ*, 504, 405
- Shao, L., Fan, Y.-Z., Wei, D.-M. 2010, *ApJ*, 719, L172
- Ukwatta, T. N., Dhuga, K. S., Stamatikos, M., et al. 2012, *MNRAS*, 419, 614
- Wei, D.-M., & Gao, W.-H. 2003, *MNRAS*, 345, 743
- Zhang, B., & Mészáros, P. 2004, *International Journal of Modern Physics A*, 19, 2385
- Zhang, B., Zhang, B.-B., Virgili, F. J., et al. 2009, *ApJ*, 703, 1696
- Zhang, F.-W. 2008, *ApJ*, 685, 1052
- Zhang, F.-W., Qin, Y.-P., & Zhang, B.-B. 2007, *PASJ*, 59, 857
- Zhang, F.-W., Shao, L., Yan, J.-Z., & Wei, D.-M., 2012, *ApJ*, 750, 88

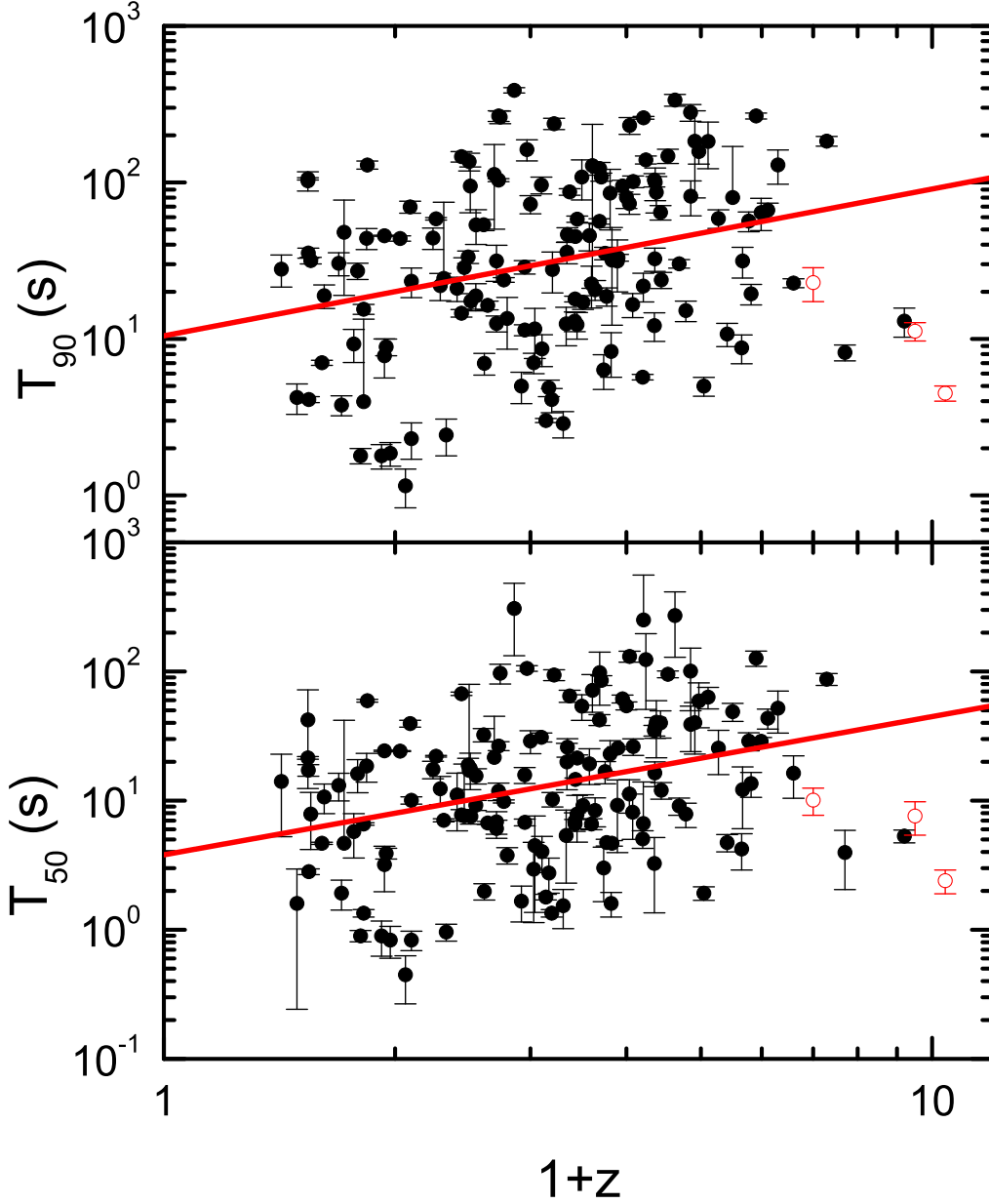


Fig. 1.— Correlations between the durations (T_{90} and T_{50} measured in the observed energy range of $140/(1+z) - 350/(1+z)$ keV) and redshift. The solid lines are our best fits: in the upper panel, we have $T_{90} = 10.5(1+z)^{0.94}$ with $r = 0.29$ and $p = 0.0005$; in the lower panel, we have $T_{50} = 3.8(1+z)^{1.07}$ with $r = 0.32$ and $p = 0.0001$. Three high redshift candidates (GRBs 090429B, 120521C, and 120923A) are also presented (open circles).

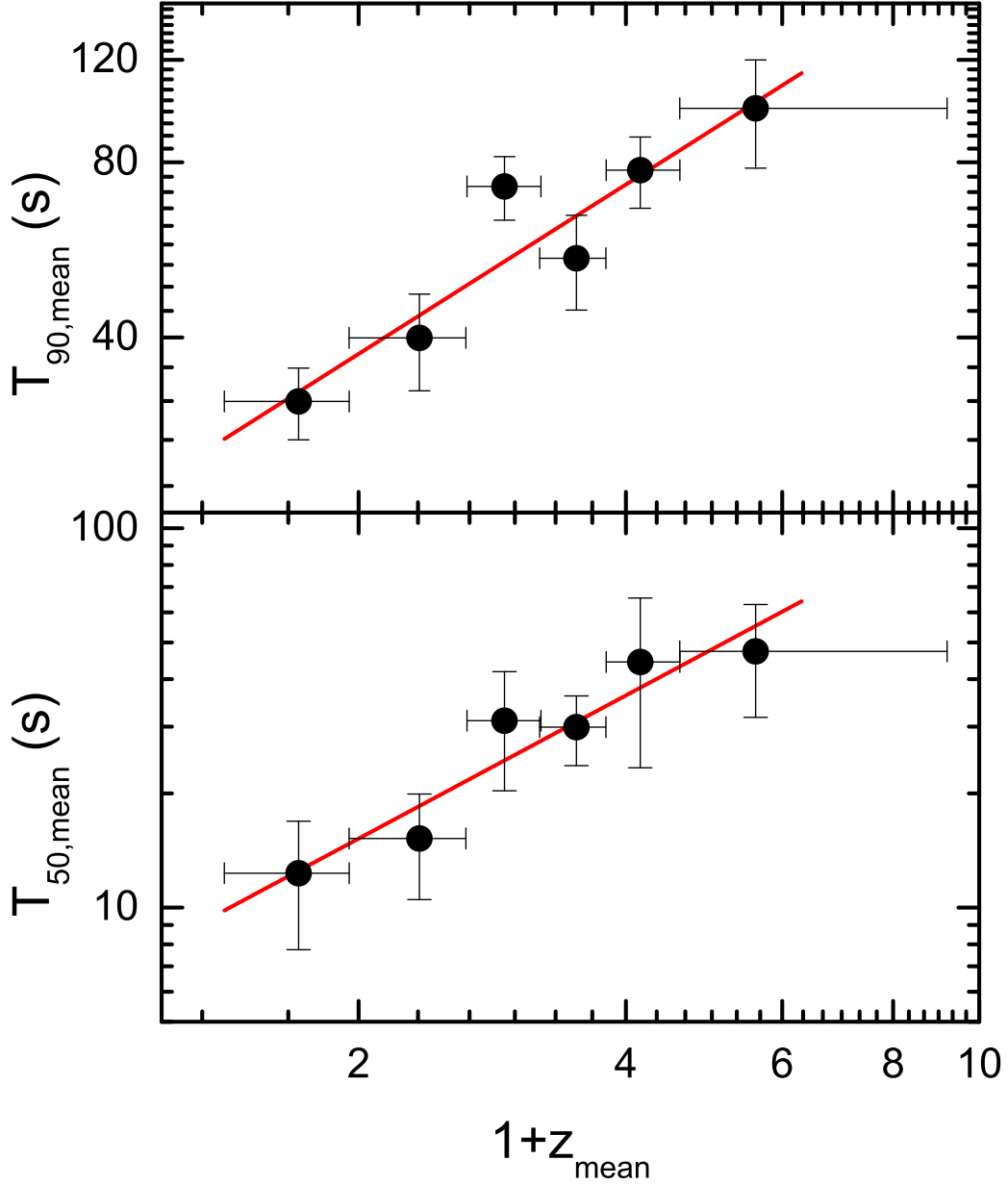


Fig. 2.— Correlations between the mean durations ($T_{90,\text{mean}}$ and $T_{50,\text{mean}}$) and the mean redshift (z_{mean}) for six groups with almost the same number of bursts, where the errors of z_{mean} only represent the redshift range in each group. The solid lines are our best fits: $T_{90,\text{mean}} = 19.1(1 + z_{\text{mean}})^{0.97}$ with $r = 0.93$ and $p = 0.007$ (upper panel) and $T_{50,\text{mean}} = 6.3(1 + z_{\text{mean}})^{1.25}$ with $r = 0.95$ and $p = 0.004$ (lower panel).

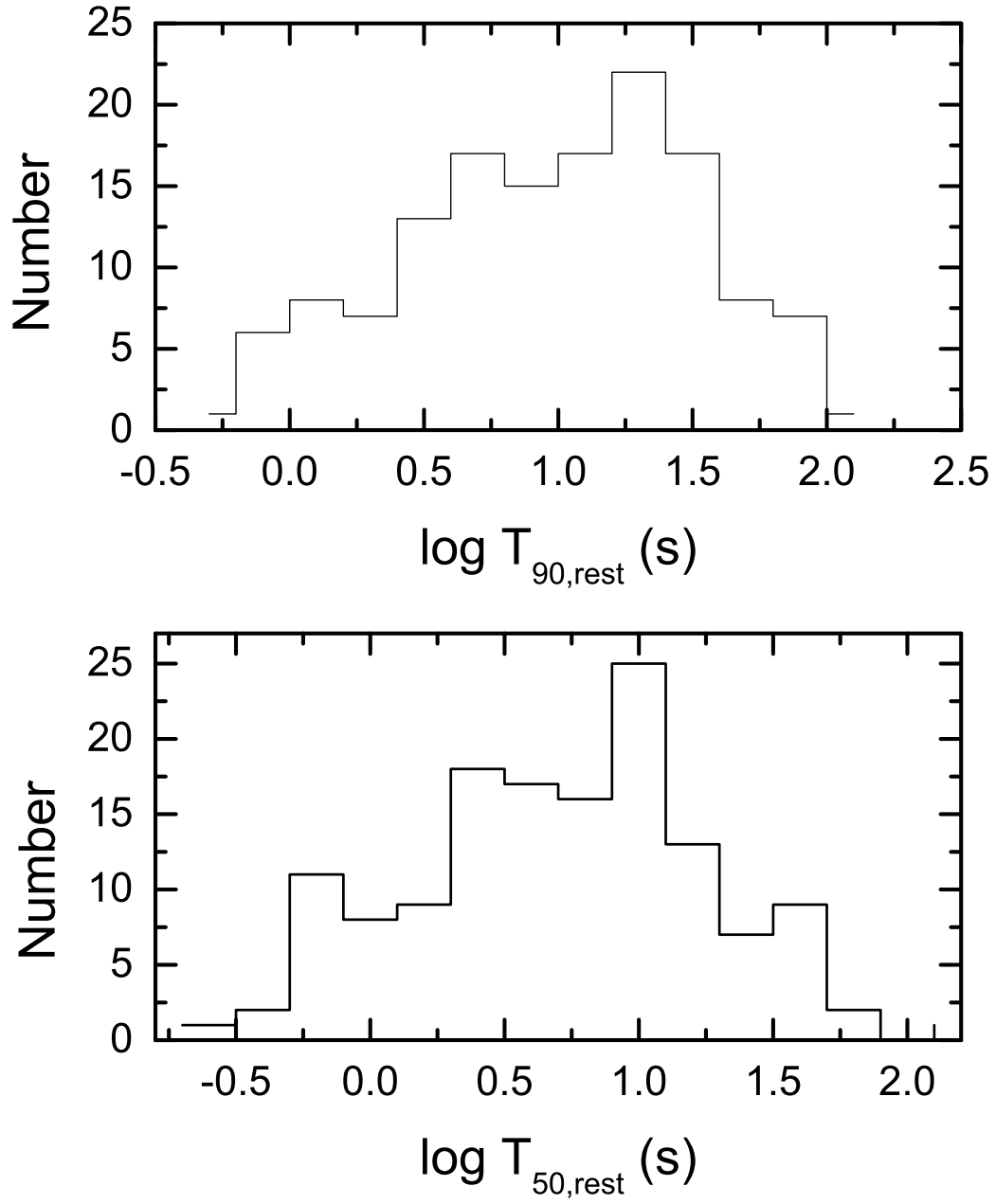


Fig. 3.— Distributions of the rest frame durations $T_{90,\text{rest}}$ and $T_{50,\text{rest}}$.

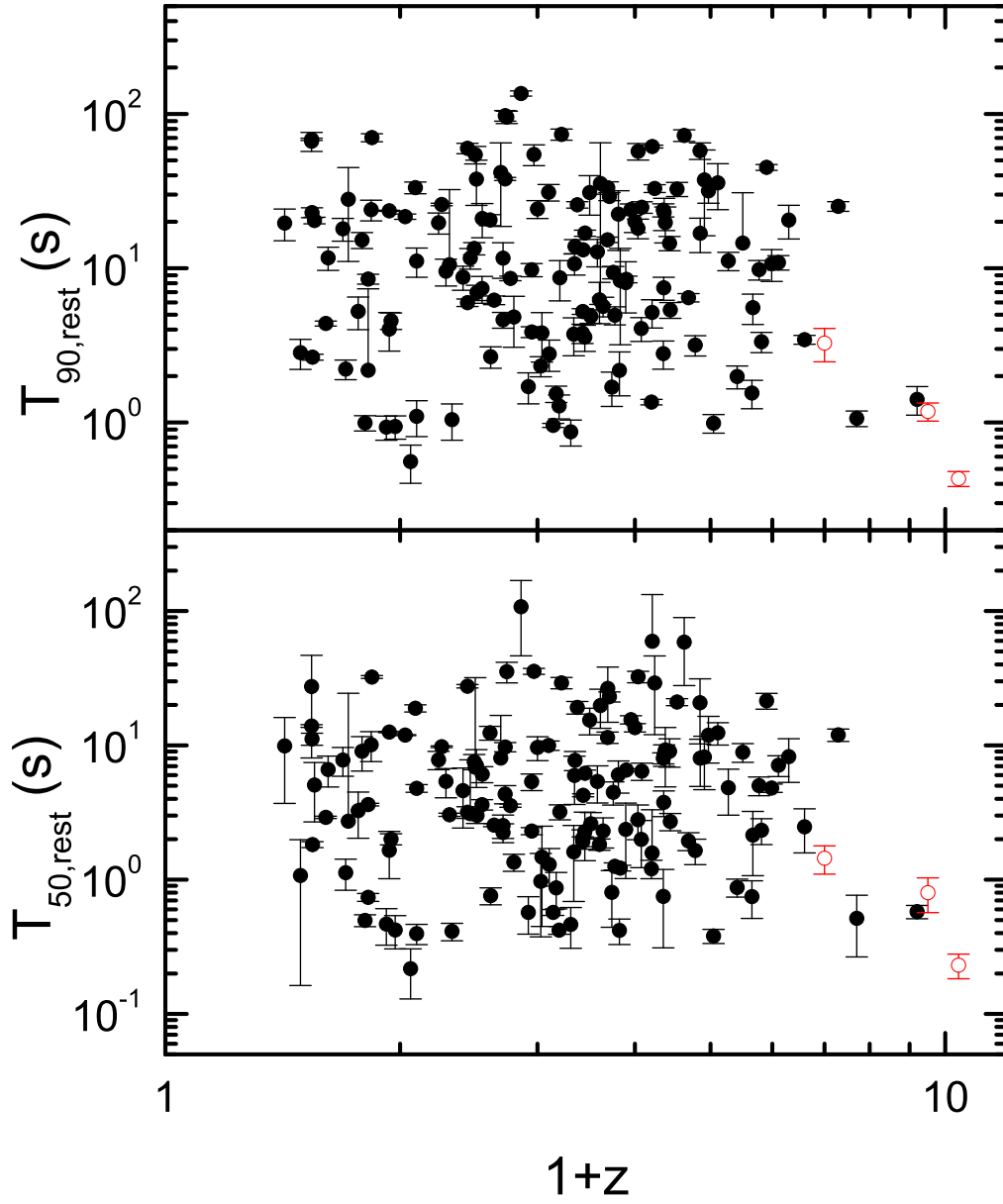


Fig. 4.— Relations between $T_{90,\text{rest}}$, $T_{50,\text{rest}}$ and redshift. Other symbols are the same as Fig. 1.

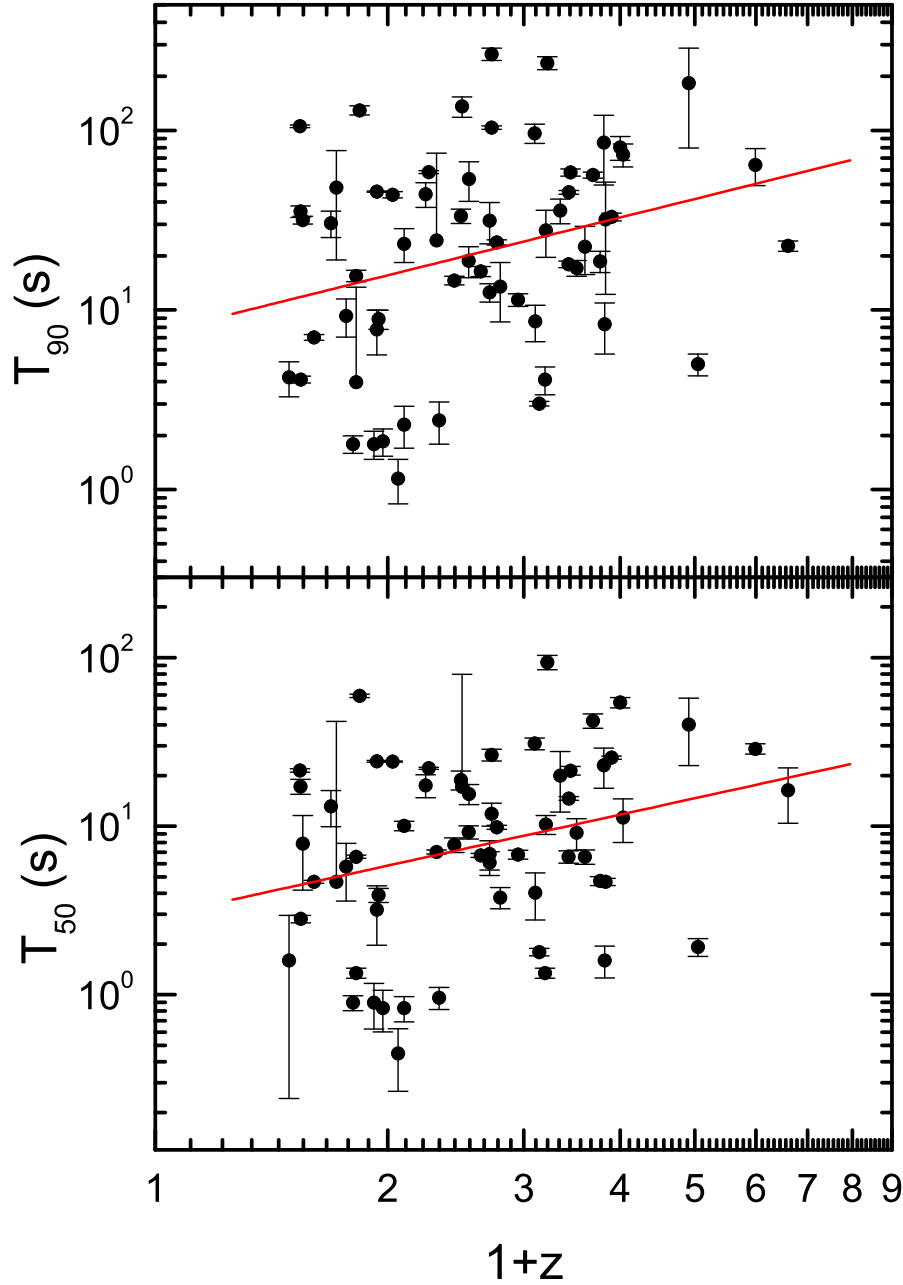


Fig. 5.— Correlations between the durations (T_{90} and T_{50}) and redshifts for 63 relatively bright GRBs with 1-s peak photon flux $P \geq 2.6 \text{ ph s}^{-1} \text{ cm}^{-2}$ in the 15-150 keV energy bands. The solid lines are our best fits: in the upper panel, we have $T_{90} = 7.4(1+z)^{1.07}$ with $r = 0.29$ and $p = 0.02$; in the lower panel, we have $T_{50} = 2.9(1+z)^{1.01}$ with $r = 0.29$ and $p = 0.02$.

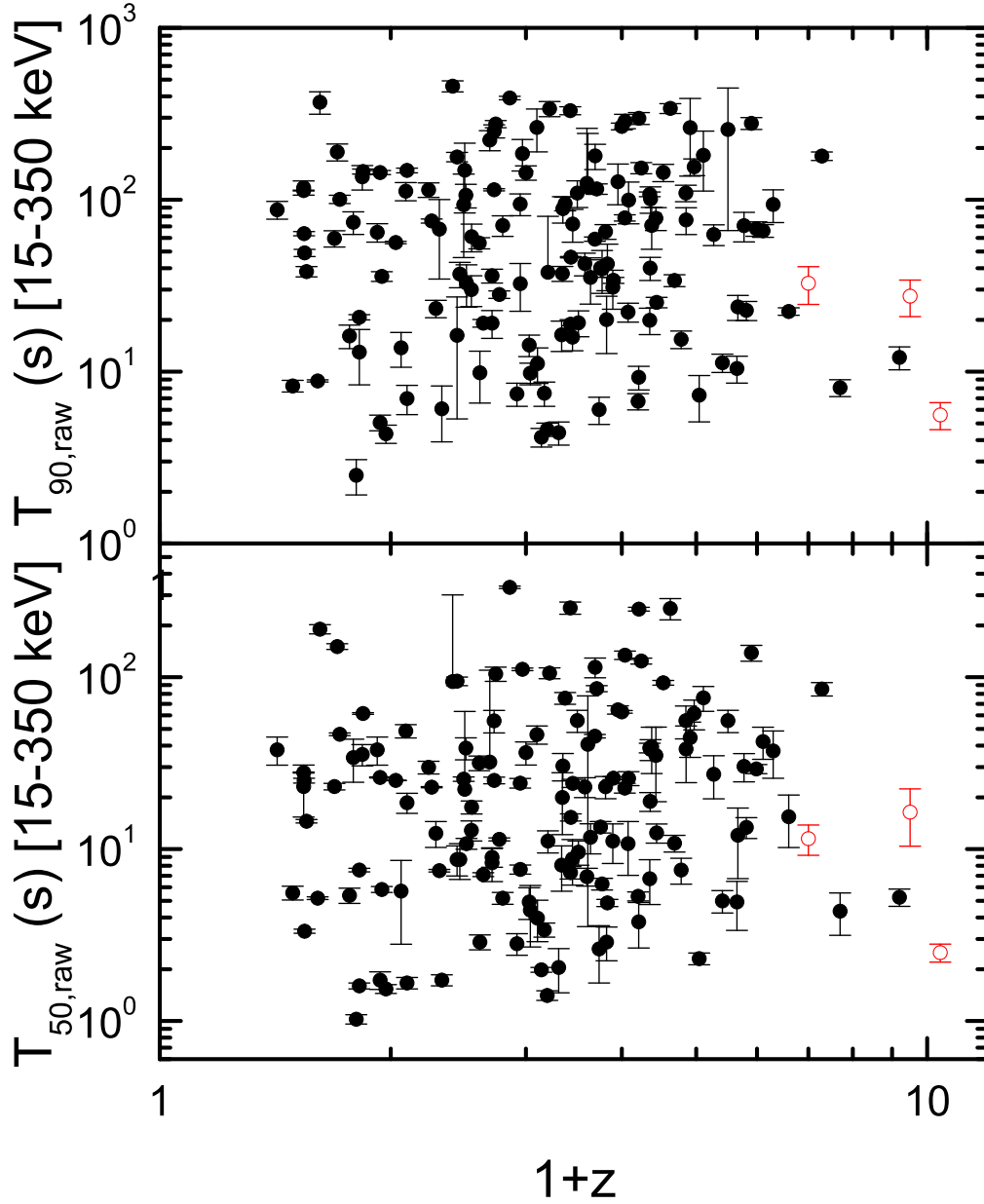


Fig. 6.— Relations between the raw duration ($T_{90,raw}$ and $T_{50,raw}$) and redshift for 139 BAT long GRBs with known redshift. The values of $T_{90,raw}$ and $T_{50,raw}$ are calculated directly in the BAT detector energy range 15-350 keV. Other symbols are the same as Fig. 1.

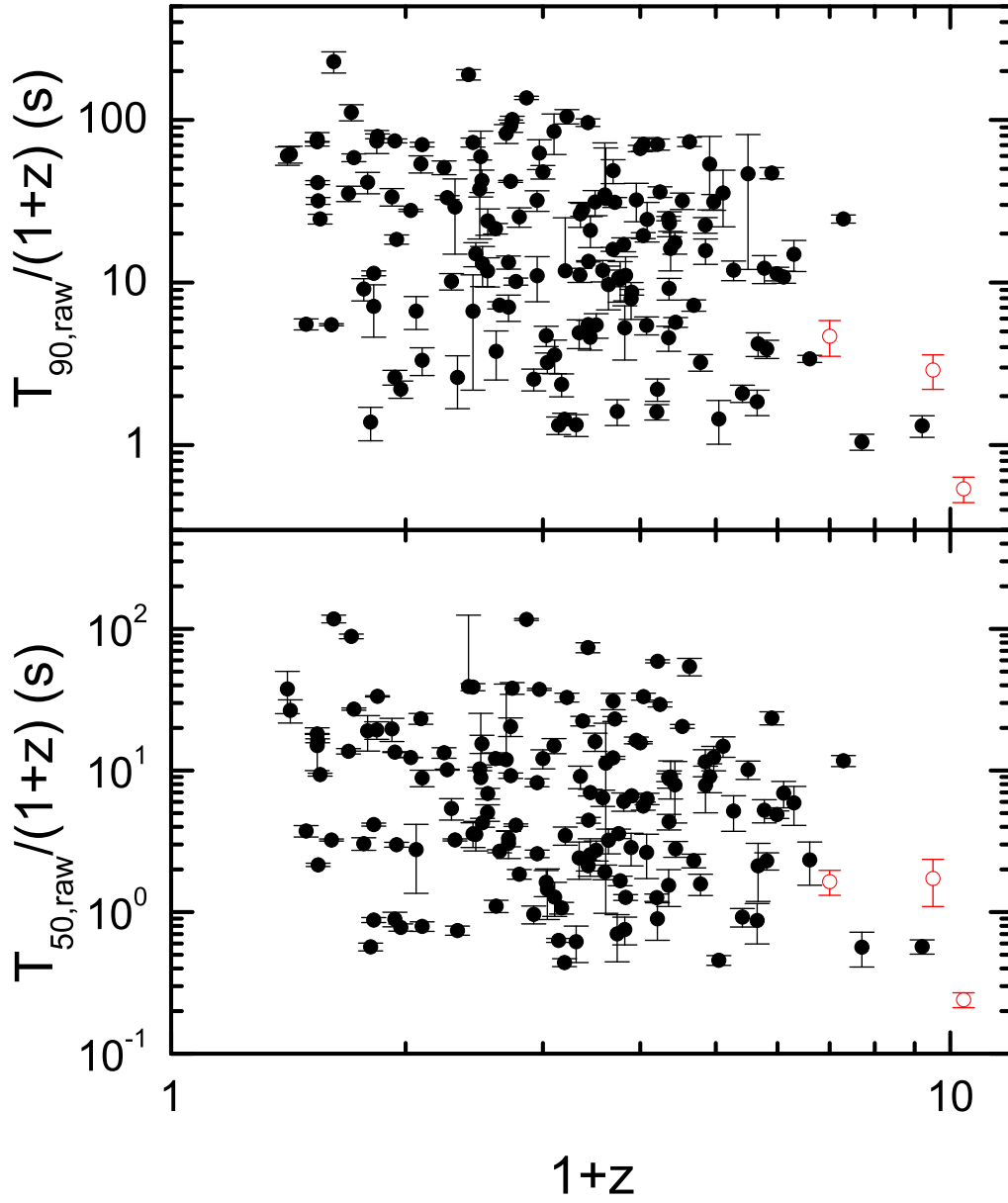


Fig. 7.— Correlations between the raw durations ($T_{90,\text{raw}}/(1+z)$ and $T_{50,\text{raw}}/(1+z)$) in the rest frame and redshift. Other symbols are the same as Fig. 1.

Table 1. Durations of 142 Swift long GRBs with known redshift*

GRB name	Obs ID	z	$T_{90,raw}$ (s)	$T_{50,raw}$ (s)	E_1^* keV	E_2^* keV	T_{90} (s)	T_{50} (s)
050126	103780	1.29	23.3±2.7	12.4±2.1	61	153	21.9±4.3	12.4±3.0
050315	111063	1.949	94.5±13.7	24.2±1.5	47	119	28.8±2.8	15.8±2.2
050318	111529	1.44	16.3±10.9	8.7±1.7	57	143	14.6±0.8	7.7±0.8
050319	111622	3.24	153.0±11.4	124.2±4.9	33	83	139.4±8.2	123.6±72.7
050401	113120	2.9	34.0±1.4	25.9±0.5	36	90	33.0±1.6	25.5±0.6
050505	117504	4.27	62.8±8.7	27.3±7.7	27	66	58.8±8.0	25.5±9.6
050525A	130088	0.606	8.8±0.1	5.2±0.1	87	218	7.0±0.3	4.7±0.1
050603	131560	2.821	20.1±7.4	2.9±0.6	37	92	8.3±2.6	1.6±0.3
050730	148225	3.97	155.5±17.3	61.5±12.1	28	70	157.6±26.6	59.2±22.5
050802	148646	1.71	19.1±3.5	8.3±1.8	52	129	12.5±1.5	6.1±1.0
050803	148833	0.422	87.5±10.4	37.8±7.0	98	246	27.9±6.5	14.1±8.8
050814	150314	5.3	94.0±20.3	37.2±11.4	22	56	129.3±31.9	52.0±18.6
050820A	151207	2.612	118.6±124.5	40.7±37.2	39	97	128.0± 106.9	71.5±23.1
050904	153514	6.29	179.5±10.3	85.4±7.6	19	48	183.6±13.2	87.2±9.2
050908	154112	3.35	19.9±3.5	6.7±2.0	32	80	12.2±2.5	3.3±1.9
050922C	156467	2.198	4.6±0.4	1.4±0.1	44	109	4.1±0.7	1.3±0.1
051109A	163136	2.346	37.2±3.7	21.2±8.4	42	105	35.8±5.6	20.0±7.8
051111	163438	1.549	61.0±11.2	17.5±1.5	55	137	53.6±13.4	15.6±2.1
060108	176453	2.03	14.3±2.0	4.9±1.0	46	116	7.0±1.0	2.9±1.8
060115	177408	3.53	144.1±16.6	92.8±2.9	31	77	147.5±15.4	95.2±5.7
060206	180455	4.045	7.3±2.2	2.3±0.2	28	69	5.0±0.7	1.9±0.2
060210	180977	3.91	263.0±125.6	44.5±10.3	29	71	183.3± 103.6	40.2±17.3
060223A	192059	4.41	11.3±1.4	5.0±0.7	26	65	10.8±1.8	4.7±0.7
060418	205851	1.489	93.6±47.5	25.5±0.7	56	141	33.4±3.1	18.8±2.4
060502A	208169	1.51	32.8±9.1	10.8±0.8	56	139	17.5±2.0	7.6±1.0
060510B	209352	4.9	278.3±22.1	138.6±14.7	24	59	265.9±11.7	126.7±17.1
060522	211117	5.11	66.0±5.6	42.2±9.0	23	57	66.6±7.1	43.5±7.7
060526	211957	3.21	297.9±23.6	248.8±6.3	33	83	258.8±5.4	250.8±308.0
060602A	213180	0.787	73.9±11.1	34.0±9.6	78	196	27.2±3.2	16.1±4.6
060605	213630	3.78	15.4±1.8	7.6±1.3	29	73	15.2±2.3	7.9±1.7
060607A	213823	3.082	99.6±27.2	25.8±2.4	34	86	101.3±8.7	26.2±3.9
060707	217704	3.43	78.1±11.9	35.1±16.2	32	79	64.3±6.8	40.0±9.5
060708	217805	1.92	7.4±1.1	2.8±0.4	48	120	5.0±1.1	1.7±0.5
060714	219101	2.71	115.6±8.1	85.8±3.5	38	94	108.2±6.4	85.4±7.4
060729	221755	0.54	117.6±11.2	23.1±7.7	91	227	102.5±14.4	42.2±29.8
060814	224552	0.84	146.0±4.9	61.5±0.7	76	190	129.3±7.7	59.4±1.5
060904B	228006	0.703	189.7±21.5	150.8±5.7	82	206	3.8±0.6	1.9±0.5
060906	228316	3.685	33.9±2.7	10.8±1.2	30	75	30.2±1.9	9.1±1.4
060908	228581	2.43	18.9±1.2	7.3±0.6	41	102	18.0±0.8	6.6±0.6
060912A	229185	0.937	5.1±0.5	1.7±0.2	72	181	7.8±2.2	3.2±1.2
060926	231231	3.208	9.3±1.5	3.8±1.1	33	83	21.8±4.5	6.7±7.3
060927	231362	5.6	22.4±1.1	15.4±5.2	21	53	22.7±1.5	16.3±5.9
061007	232683	1.261	75.3±2.1	22.9±0.2	62	155	58.6±1.1	22.1±0.3
061110B	238174	3.44	25.3±1.8	12.4±1.6	32	79	23.8±2.8	12.0±1.8
061121	239899	1.314	67.5±32.9	7.5±0.1	61	151	24.4±50.4	7.0±0.2

Table 1—Continued

GRB name	Obs ID	z	$T_{90,raw}$ (s)	$T_{50,raw}$ (s)	E_1^* keV	E_2^* keV	T_{90} (s)	T_{50} (s)
061222B	252593	3.355	40.1±6.1	18.9±2.4	32	80	32.5±5.5	16.4±3.6
070110	255445	2.352	88.7±15.5	30.5±5.5	42	104	46.5±4.9	25.9±4.2
070306	263361	1.497	148.5±64.7	22.3±41.0	56	140	136.1±17.7	17.2±62.5
070318	271019	0.836	136.0±22.0	35.5±5.0	76	191	44.0±6.7	18.6±4.7
070411	275087	2.954	127.4±33.9	64.6±3.6	35	89	95.0±8.2	61.4±4.3
070506	278693	2.31	4.4±0.7	2.0±0.6	42	106	2.9±0.6	1.5±0.5
070508	278854	0.82	20.7±0.7	7.6±0.2	77	192	15.5±1.1	6.6±0.1
070521	279935	0.553	38.2±2.7	14.5±0.3	90	225	31.7±1.5	7.9±3.7
070529	280706	2.4996	109.4±19.4	55.9±8.2	40	100	108.3±31.1	54.0±12.1
070611	282003	2.04	9.8±1.4	4.4±1.7	46	115	11.6±4.1	4.5±3.1
070612A	282066	0.617	369.4±55.0	190.3±11.8	87	216	18.9±3.2	10.7±2.8
070714B	284856	0.92	64.6±7.9	37.8±7.0	73	182	1.8±0.3	0.9±0.3
070721B	285654	3.626	339.9±22.2	251.0±35.5	30	76	336.0±29.1	271.4±142.6
070802	286809	2.45	15.9±2.6	8.8±2.6	41	101	12.4±2.4	7.9±3.1
070810A	287364	2.17	7.5±1.2	3.4±0.3	44	110	4.9±0.6	2.8±0.8
071003	292934	1.1	148.1±4.7	18.6±2.5	67	167	23.4±5.0	10.0±0.7
071010B	293795	0.947	35.8±2.3	5.8±0.2	72	180	8.9±1.1	3.9±0.4
071020	294835	2.142	4.2±0.5	2.0±0.1	45	111	3.0±0.1	1.8±0.1
071031	295670	2.692	180.1±30.2	114.2±15.0	38	95	122.8±11.4	98.0±43.2
071117	296805	1.331	6.1±2.2	1.7±0.1	60	150	2.4±0.6	1.0±0.1
080207	302728	1.74	275.6±13.1	104.5±9.9	51	128	261.5±24.2	96.9±16.9
080210	302888	2.641	35.3±10.6	11.7±2.3	38	96	20.6±3.0	8.4±2.1
080310	305288	2.4266	330.2±17.6	252.9±20.5	41	102	13.0±1.9	6.9±1.1
080319B	306757	0.937	144.0±4.0	26.1±0.2	72	181	45.6±0.4	24.3±0.3
080319C	306778	1.95	32.5±10.0	7.6±0.5	47	119	11.4±0.9	6.8±0.4
080411	309010	1.03	56.4±0.9	25.1±0.1	69	172	43.8±1.7	24.2±0.2
080413A	309096	2.433	46.3±0.4	15.3±0.7	41	102	45.2±1.1	14.6±0.4
080413B	309111	1.1	7.0±1.4	1.7±0.1	67	167	2.3±0.6	0.8±0.1
080430	310613	0.767	16.1±2.5	5.4±0.5	79	198	9.3±2.2	5.8±2.2
080516	311762	3.2	6.7±0.7	5.3±0.3	33	83	5.7±0.2	5.1±0.8
080603B	313087	2.69	59.0±1.7	45.4±1.1	38	95	56.4±2.3	42.2±4.1
080605	313299	1.6398	19.1±1.0	7.1±0.2	53	133	16.4±1.0	6.7±0.2
080607	313417	3.036	78.5±3.3	22.7±1.5	35	87	73.3±10.7	11.3±3.3
080721	317508	2.602	124.6±135.8	6.9±0.8	39	97	22.5±6.7	6.6±0.6
080804	319016	2.2045	37.8±42.3	11.1±1.6	44	109	27.8±8.1	10.2±1.3
080805	319036	1.505	106.3±16.7	38.7±5.7	56	140	94.8±30.8	17.7±5.6
080810	319584	3.35	107.6±3.3	38.8±2.5	32	80	103.7±10.1	34.9±3.3
080905B	323898	2.374	94.9±8.6	75.5±5.9	41	104	87.0±4.2	64.6±6.9
080906	323984	2	143.7±13.7	36.4±5.6	47	117	72.6±9.7	28.9±5.8
080913	324561	6.7	8.1±0.9	4.4±1.2	18	45	8.2±1.0	4.0±1.9
080916A	324895	0.689	59.6±6.5	23.1±1.0	83	207	30.4±5.1	13.1±3.2
080928	326115	1.692	222.5±29.7	32.1±77.8	52	130	112.5±62.2	21.6±23.3
081008	331093	1.9685	185.7±38.6	111.1±1.9	47	118	162.2±25.0	105.7±5.3
081028A	332851	3.038	286.5±27.6	134.3±7.6	35	87	231.2±28.3	130.9±12.8
081029	332931	3.8479	109.4±12.1	55.9±12.1	29	72	280.3±34.3	100.7±51.1

Table 1—Continued

GRB name	Obs ID	z	$T_{90,raw}$ (s)	$T_{50,raw}$ (s)	E_1^* keV	E_2^* keV	T_{90} (s)	T_{50} (s)
081118	334877	2.58	42.5±6.4	23.0±3.0	39	98	45.8±9.2	19.3±5.9
081121	335105	2.512	19.3±3.3	9.6±1.5	40	100	17.2±1.7	9.2±1.9
081203A	336489	2.1	263.6±73.6	46.4±5.6	45	113	96.3±11.8	30.9±2.5
081222	337914	2.77	39.6±11.1	6.3±0.5	37	93	18.7±2.5	4.7±0.3
090102	338895	1.547	30.0±6.1	12.9±1.7	55	137	18.8±3.7	9.2±0.8
090205	342121	4.6497	10.4±1.9	4.9±1.6	25	62	8.8±1.8	4.2±1.3
090313	346386	3.375	70.9±19.4	39.4±11.9	32	80	86.5±22.7	40.4±19.0
090418A	349510	1.608	56.0±4.2	31.7±3.1	54	134	53.6±4.4	32.3±3.8
090423	350184	8.2	12.1±1.8	5.2±0.6	15	38	13.0±2.7	5.3±0.6
090424	350311	0.544	49.1±2.4	3.3±0.1	91	227	4.1±0.2	2.8±0.1
090516A	352190	4.109	181.6±69.3	75.8±12.5	27	69	182.8±60.3	63.4±12.0
090519	352648	3.85	76.3±13.6	38.2±13.8	29	72	81.7±20.5	38.9±15.0
090618	355083	0.54	113.1±0.6	27.9±0.2	91	227	105.5±1.7	21.4±0.5
090715B	357512	3	267.0±12.0	62.8±1.1	35	88	80.3±12.1	54.2±3.9
090809	359530	2.737	6.0±1.1	2.6±1.0	37	94	6.3±1.6	3.0±1.4
090812	359711	2.452	72.3±15.6	24.1±1.3	41	101	58.3±2.7	21.4±1.2
090926B	370791	1.24	114.2±11.1	29.9±2.5	63	156	44.2±6.9	17.5±2.7
091018	373172	0.971	4.4±0.5	1.5±0.1	71	178	1.9±0.3	0.8±0.2
091020	373458	1.71	36.1±3.3	9.0±1.1	52	129	31.5±8.2	6.8±1.4
091024	373674	1.092	112.3±13.6	48.6±4.3	67	167	69.7±6.1	39.5±2.4
091029	374210	2.752	40.1±4.7	13.4±1.0	37	93	35.3±3.2	16.8±3.3
091109A	375246	3.076	22.2±2.8	10.8±3.7	34	86	16.6±2.9	8.1±3.1
091127	377179	0.49	8.3±0.6	5.6±0.5	94	235	4.2±0.9	1.6±1.4
091208B	378559	1.063	13.8±3.2	5.7±2.9	68	170	1.2±0.3	0.4±0.2
100219A	412982	4.6667	23.8±4.0	12.0±5.3	25	62	31.5±7.0	12.2±6.1
100302A	414592	4.813	22.7±2.9	13.4±1.9	24	60	19.4±2.9	13.6±3.0
100513A	421814	4.772	70.7±13.8	30.3±5.6	24	61	56.6±8.2	28.9±4.6
100621A	425151	0.542	63.5±1.8	25.0±0.8	91	227	35.4±2.6	17.2±1.8
100728B	430172	2.106	11.1±2.6	4.0±1.1	45	113	8.6±2.0	4.0±1.3
100814A	431605	1.44	177.4±11.2	94.8±5.4	57	143	146.1±11.2	67.3±2.0
100816A	431764	0.8034	2.5±0.6	1.0±0.1	78	194	1.8±0.2	0.9±0.1
100901A	433065	1.408	457.7±33.9	94.3±206.7	58	145	21.1±3.7	11.1±5.2
100902A	433160	4.5	256.6±190.4	55.9±8.3	25	64	80.1±89.6	48.9±7.8
100906A	433509	1.727	114.3±1.6	55.7±8.3	51	128	103.4±2.3	11.8±1.8
110128A	443861	2.339	16.4±3.3	8.1±2.4	42	105	12.5±3.4	5.4±3.1
110205A	444643	2.22	338.4±34.2	105.7±7.6	43	109	237.3±19.7	94.0±9.1
110213A	445414	1.46	37.0±6.2	8.7±2.0	57	142	28.6±4.4	7.6±11.6
110422A	451901	1.77	28.1±1.4	11.4±0.2	51	126	23.8±0.8	9.9±0.3
110503A	452685	1.613	9.9±3.3	2.9±0.3	54	134	7.0±1.1	2.0±0.3
110715A	457330	0.82	13.0±4.6	1.6±0.1	77	192	4.0±9.4	1.3±0.1
110731A	458448	2.83	42.4±12.8	4.9±0.2	37	91	31.9±19.6	4.7±0.2
110801A	458521	1.858	390.8±9.1	333.2±5.4	49	122	388.1±15.1	307.6±175.1
110818A	500914	3.36	101.1±17.7	38.0±5.3	32	80	100.1±23.6	37.2±6.8
111008A	505054	4.9898	67.8±6.5	29.2±1.8	23	58	64.1±14.9	28.8±2.0
111107A	507185	2.893	31.0±7.9	11.1±2.9	36	90	31.4±11.5	9.2±5.3

Table 1—Continued

GRB name	Obs ID	z	$T_{90,raw}$ (s)	$T_{50,raw}$ (s)	E_1^* keV	E_2^* keV	T_{90} (s)	T_{50} (s)
111228A	510649	0.716	100.6±5.6	46.6±0.8	82	204	48.1±29.1	4.7±37.3
120119A	512035	1.728	250.8±21.9	25.1±1.1	51	128	266.0±20.9	26.5±2.1
120326A	518626	1.798	70.9±9.7	5.2±0.4	50	125	13.5±4.9	3.8±0.5
120327A	518731	2.81	65.3±6.4	23.0±3.4	37	92	85.4±35.7	23.0±6.2
090429B	350854	~9.4	5.6±1.0	2.5±0.3	13	34	4.5±0.5	2.4±0.5
120521C	522656	~6.0	32.7±8.1	11.5±2.3	20	50	22.9±5.6	10.1±2.4
120923A	534402	~8.5	27.5±6.6	16.4±6.0	15	37	11.2±1.5	7.6±2.2

Available in the electronic version only.

* E_1 and E_2 correspond to the lower ($140/(1+z)$) and upper ($350/(1+z)$) limit of energy range used to measure durations T_{90} and T_{50} .